Topological Crystalline Insulators and Topological Superconductors: From Concepts to Materials

Yoichi Ando[1] and Liang Fu[2]
[1]*Institute of Scientific and Industrial Research, Osaka University, Ibaraki, Osaka 567-0047, Japan*
[2]*Department of Physics, Massachusetts Institute of Technology, Cambridge, MA 02139, USA*

Key Words Topological Crystalline Insulator, Topological Superconductor, Dirac Fermions

Abstract
In this review, we discuss recent progress in the explorations of topological materials beyond topological insulators; specifically, we focus on topological crystalline insulators and bulk topological superconductors. The basic concepts, model Hamiltonians, and novel electronic properties of these new topological materials are explained. The key role of symmetries that underlie their topological properties is elucidated. Key issues in their materials realizations are also discussed.

CONTENTS

1 Introduction

In the past decade, there has been remarkable progress in our understanding of topological states of matter. A quantum state may be called topological when its wavefunctions bear a distinct character that can be specified by some topological invariant—a discrete quantity that remains unchanged upon adiabatic deformations of the system. Materials realizing such topological states in their bulk may be called topological materials. Since the 1980s, quantum Hall systems (1) and superfluid Helium 3 (He-3) (2) have been recognized to be topological, but it was long believed that such topological states are rather exceptional in nature and exist only in quantum liquids under extreme conditions (under high magnetic fields or at low temperatures). However, after the discovery of topological insulators (TIs) (3, 4, 5, 6, 7, 8, 9, 10, 11, 12, 13), it has come to be widely recognized that topological states of matter can actually be widespread. In this sense, TIs have established a new paradigm about topological materials. It is generally expected that studies of topological materials would deepen our understanding of quantum mechanics in solids in a fundamental way.

By now, the theoretical aspect of TIs are reasonably well understood; hence, major challenges on the theoretical front concerns expansions of our notion of topological materials. On the experimental front, however, TIs are still far from being sufficiently investigated; materials issues in three-dimensional (3D) TIs are being solved (13), and there are serious on-going efforts to realize theoretically predicted novel phenomena, such as topological magnetoelectric effects (14) and proximity-induced topological superconductivity hosting the non-Abelian Majorana zero mode in the vortex core (15). At the same time, new materials discoveries are still crucially important in this rapidly developing field, and the search for new types of topological materials is in progress worldwide (13).

In this review, we mainly focus on two new classes of topological phases of matter beyond TIs, namely, topological crystalline insulators (TCIs) and topological superconductors (TSCs). The basic concepts and effective models are concisely summarized, so that experimentalists can grasp the essential physics of these topological matters to accomplish new material discoveries. We also discuss actual (candidate) materials for each category and mention the issues to be addressed in future studies.

1.1 Z_2 Topological Insulator

Before going into the main topics of this review, TCIs and TSCs, let us briefly summarize the current status of the TI research. As the first class of materials identified to exhibit topological properties preserving time-reversal symmetry, TIs are characterized by the topological invariant called the Z_2 index (3, 16). The concept and definition of the Z_2 index are pedagogically summarized in a recent review article (13). Lately, theoretical works on TIs are mostly focused on either the effects of electron interactions or the phenomenological consequences

of its topological character. On the materials front, all TI materials confirmed to date are narrow-gap semiconductors with an inverted band gap (13). Such band inversions must occur at an odd number of time-reversal-invariant momenta (TRIMs) to obtain a nontrivial Z_2 index. Both two-dimensional (2D) and 3D TI materials have been studied, and the materials efforts can be summarized as follows.

Among 2D systems, there are two cases that have been confirmed to be 2D TIs. Those two 2D TI systems are both realized in artificial quantum well structure and the band inversion takes place at the center of the Brillouin zone, i.e. at the Γ point. The first system confirmed to be a 2D TI was a thin layer of HgTe sandwiched by CdTe (4, 5), and the second one was InAs/GaSb heterojunction sandwiched by AlSb (17, 18). In HgTe, the band inversion is naturally realized due to the large spin-orbit coupling stemming from the heavy element Hg, but the cubic symmetry of this material causes the valence and conduction bands to be degenerate at the Γ point; the quantum confinement and the resulting formation of subbands removes this degeneracy and leads to the realization of a true 2D TI state. In InAs/GaSb heterojunction, however, the band inversion is achieved by the broken (type-III) gap alignment between InAs and GaSb, and the band gap in the hybridized band structure is created by the anticrossing of the inverted electron and hole subbands stemming from InAs and GaSb, respectively. Experimentally, although the materials are difficult to grow in both cases, it is relatively easy to make the transport through the helical edge states to become predominant in those 2D TIs by using electrostatic gating.

Among 3D materials, the first one to be confirmed as 3D TI was $Bi_{1-x}Sb_x$ alloy (9, 10). In this material, the band inversion occurs at three TRIMs, the L points; the surface band structure is rather complicated, consisting of an odd number of Dirac cones and additional states (10, 19). Other 3D TI materials found to date have the band inversion only at the Γ point, and hence they are associated with simpler surface band structures consisting of a single Dirac cone. Among such simpler 3D TI materials, the most widely studied are the binary tetradymite compounds Bi_2Se_3 and Bi_2Te_3 (20, 21, 22), in which the band inversion is due to a strong spin-orbit coupling that switches the order of two p_z-orbital-dominated bands with opposite parities at the Γ point.

Unfortunately, most of the known 3D TI materials are not really insulating in the bulk due to unintentional doping. Hence, an important experimental issue has been to find suitable materials that present sufficiently high bulk resistivity so that the surface transport properties can be reliably probed (13). In this regard, the ternary tetradymite compound Bi_2Te_2Se was the first material that achieved a reasonably large bulk resistivity with a high surface mobility, allowing clear observations of surface quantum oscillations (23, 24). Later, in an alloyed tetradymite compound $Bi_{2-x}Sb_xTe_{3-y}Se_y$, a series of special compositions to achieve minimal bulk conduction was identified (25), and the surface-dominated transport was demonstrated for the first time in bulk single crystals of a 3D TI (26). In thin films of 3D TIs, similar surface-dominated transport has been achieved in strained HgTe (27) and in $Bi_{2-x}Sb_xTe_3$ (28). Also, in exfoliated thin

flakes of Bi_2Se_3, it was reported that the deposition of strongly electron-affine molecules called F4TCNQ makes it possible to achieve the surface-dominated transport (29). With those advancements in materials, experimental studies of the intrinsic properties of 3D TIs have become possible.

1.2 Symmetry-Protected Topological Phases

The advent of TIs draws wide attention to the broad notion of symmetry-protected topological (SPT) phases (30), of which TI is an example. Generally speaking, a SPT phase exhibits topological characteristics (e.g., topological invariants and gapless boundary states) that rely crucially on the presence of certain symmetry (e.g., time reversal symmetry), and it can be adiabatically deformed to a trivial phase (e.g., an atomic insulator) after this underlying symmetry is removed. In recent years, the search for other SPT phases has attracted tremendous activities on both theoretical and experimental sides (31). The two new topological phases treated in this review, i.e. TCIs and TSCs, are subsets of SPT phases, and for both of them several material realizations/candidates are currently under study. Similar to TIs, TCIs and TSCs are defined by topological invariants encoded in the wavefunctions of Bloch electrons and of Bogoliubov quasiparticles, respectively.

2 Topological Crystalline Insulator

2.1 General Concept

TCIs (TCIs) (32) are topological phases of matter that are protected by crystal symmetries, including rotation, reflection, etc.; for example, C_{3v} point group requires threefold rotation and reflection symmetries. A TCI cannot be adiabatically deformed to an atomic insulator while preserving certain crystal symmetry. Several theoretical examples of such crystal-symmetry-protected topological phases have been studied in the context of TIs (3, 6, 7, 33) and related systems (34). A systematic search for TCIs requires the classification of topologically distinct band structures within each crystal class. Given the richness and complexity of crystallography, the full classification of TCI has not yet been attained and is an active area of current research. In this review, we largely focus on a class of TCIs that has been experimentally realized (35, 36, 37, 38), whose topological character is protected by reflection symmetry with respect to a crystal plane, or equivalently, mirror symmetry.

Reflection M is equal to a product of spatial inversion P and the two-fold rotation C_2 around the axis perpendicular to the plane of reflection (hereafter denoted by $z = 0$): $M = PC_2$. In spin-orbit-coupled systems, C_2 is a combined rotation of an electron's spatial coordinates and spin. Thus reflection acts on a spinful wavefunction as follows

$$M \begin{pmatrix} \psi_\uparrow(\mathbf{r}) \\ \psi_\downarrow(\mathbf{r}) \end{pmatrix} = \begin{pmatrix} -i\psi_\uparrow(\bar{\mathbf{r}}) \\ i\psi_\downarrow(\bar{\mathbf{r}}) \end{pmatrix}, \tag{1}$$

where $\bar{\mathbf{r}} = (x, y, -z)$. Note that to define M properly requires picking an orientation for the plane of reflection that distinguishes the $+z$ and $-z$ directions. Owing to the sign reversal of spinor under 2π rotation, $M^2 = -1$ and hence eigenvalues of M are either i or $-i$.

The presence of mirror symmetry in a crystal has implications for its energy eigenstates in momentum space, i.e., Bloch states $|\psi_{\mathbf{k}}\rangle$. For a 2D crystal that is invariant under $z \to -z$, $|\psi_{\mathbf{k}}\rangle$ can be chosen to be eigenstates of M for all $\mathbf{k}$. This yields two classes of Bloch eigenstates with mirror eigenvalues $\eta = \pm i$, denoted by $|\psi_{\mathbf{k},\eta}\rangle$. For each class of Bloch eigenstates, one can define a corresponding Chern numbers N_η. This leads to two independent topological invariants: the total Chern number $N \equiv N_{+i} + N_{-i}$ determines the quantized Hall conductance, and a new invariant called "mirror Chern number": $N_M \equiv (N_{+i} - N_{-i})/2$ (33). Importantly, even when the total Chern number is zero, the mirror Chern number can be a nonzero integer, which then defines a TCI phase protected by the mirror symmetry.

The above idea can be generalized to 3D crystals that have one or multiple mirror planes. The presence of a given mirror symmetry, say $x \to -x$, implies that the Bloch states $|\psi_{\mathbf{k}}\rangle$ at the $k_x = 0$ and $k_x = \pi/a$ planes in the 3D Brillouin zone are mirror eigenstates. Each such mirror-invariant plane in momentum space is then indexed by its own mirror Chern number. The complete set of mirror Chern numbers classifies 3D TCI phases with mirror symmetry.

The topological character of a TCI leads to gapless states on the boundary. Importantly, because the boundary can have lower symmetry than the bulk, not all crystal surfaces of the above 3D TCI are gapless; only those surfaces that preserve the underlying mirror symmetry are. The dependence of boundary states on surface orientations is a generic property of TCIs (32, 34) and enriches topological phenomena in solids, as we will show below.

2.2 Models and Materials

In 2012, Hsieh *et al.* (35) predicted the first class of TCI materials in IV-VI semiconductors, with SnTe as a representative. These materials crystallize in rock-salt structure. The symmetry responsible for their topological character comes from the reflection symmetry with respect to the (110) mirror planes. In stark contrast, the isostructural compound PbTe in the same IV-VI material family is predicted to be non-topological. We describe below the important difference between SnTe and PbTe in electronic structures, and its implication for TCI.

Both SnTe and PbTe have small direct band gaps located at four symmetry-related TRIMs, the L points. The low-energy band structure, consisting of the doubly degenerate conduction and valence bands in the vicinity of L, is described by a four-band $k \cdot p$ Hamiltonian $H(\mathbf{k})$ (35), which can be regarded as the low-energy limit of a microscopic six-band model in the early work of Mitchell & Wallis (39). Alternatively, in the spirit of modern condensed matter physics, $H(\mathbf{k})$ can be regarded as an effective Hamiltonian, whose analytical form can be derived entirely from the symmetry properties of energy bands. The little group that keeps each L point invariant is D_{3d}, a subgroup of the O_h point

group of the rock-salt structure. The group D_{3d} consists of three independent symmetry operations: spatial inversion (P), reflection with respect to the (110) plane (M), and three-fold rotation around the (111) axis (C_3). The conduction and valence bands at a given L point form two sets of Kramers doublets with opposite parity eigenvalues, denoted by $|\psi^+_{L,\alpha}\rangle$ and $|\psi^-_{L,\alpha}\rangle$ respectively. The two members of a Kramers doublet denoted by $\alpha = 1, 2$ have opposite total angular momenta $J_z = \pm\frac{\hbar}{2}$ respectively. Because the axis of rotation is parallel to the plane of reflection, J_z changes sign under reflection, i.e., $M|\psi^\pm_{L,1}\rangle = i|\psi^\pm_{L,2}\rangle$ and $M|\psi^\pm_{L,2}\rangle = i|\psi^\pm_{L,1}\rangle$.

The above band symmetries dictate the form of the $k \cdot p$ Hamiltonian $H(\mathbf{k})$, where $\mathbf{k}$ is measured from a given L point. $H(\mathbf{k})$ is a 4×4 matrix in the basis set of $\{|\psi^+_{L,1}\rangle, |\psi^+_{L,2}\rangle, |\psi^-_{L,1}\rangle, |\psi^-_{L,2}\rangle\}$, which is given by

$$H(\mathbf{k}) = \begin{pmatrix} m & 0 & -iv'k_z & -v(ik_x + k_y) \\ 0 & m & v(ik_x - k_y) & -iv'k_z \\ iv'k_z & -v(ik_x + k_y) & -m & 0 \\ v(ik_x - k_y) & iv'k_z & 0 & -m \end{pmatrix}. \quad (2)$$

$H(\mathbf{k})$ includes all possible terms up to first order in $\mathbf{k}$, which are invariant under the symmetry group D_{3d}. Remarkably, after a rescaling of the coordinate $k_z \to \frac{v'}{v}k_z$, $H(\mathbf{k})$ has the same form as the Dirac Hamiltonian in quantum electrodynamics: $H(\mathbf{k}) = m\Gamma_0 + v\sum_i k_i\Gamma_i$, where $\Gamma_{0,\ldots,3}$ are Dirac gamma matrices defined by $\Gamma_0 = \sigma_z \otimes I, \Gamma_1 = \sigma_x s_y, \Gamma_2 = -\sigma_x s_x$, and $\Gamma_3 = \sigma_y \otimes I$. Thus, the low-energy electronic properties of SnTe and PbTe are governed by massive Dirac fermions in 3+1 dimension. The conduction and valence bands are separated by an energy gap $E_g = 2|m|$, and have particle-hole symmetric dispersions $E_{c,v}(k) = \pm\sqrt{m^2 + v^2k^2}$.

The topological distinction between SnTe and PbTe arises from their different Dirac masses. It has long been known that in going from PbTe to SnTe, the band gap of the alloy $Pb_{1-x}Sn_xTe$ closes at a critical Sn composition, $x \sim 0.35$, and then reopens (40). This band inversion corresponds to a sign change of the Dirac mass in the low-energy theory (2). The key insight that led to the prediction of the TCI phase (35) came from the recognition that this Dirac mass reversal has an important consequence for topology: It changes the mirror Chern number N_M associated with the $k_x = 0$ plane passing through Γ and two L points, such as $\Gamma L_1 L_2$, $\Gamma L_3 L_4$ and $\Gamma L_1 L_3$ [see Fig. 1(a)]. Energy bands on these planes are mirror eigenstates indexed by $\eta = -is_x$. The simultaneous band inversions at the two L points on the $k_x = 0$ plane add up to an integer value of the mirror Chern number: $1 + 1 = 2$. Therefore, one of the two materials, SnTe or PbTe, must have a nonzero mirror Chern number $|N_M| = 2$ and thus realizes a TCI phase protected by mirror symmetry. However, neither material is a Z_2 TI (9), because an even number of band inversions "annihilate" each other, as can be seen from addition rule of the Z_2 group classification of time-reversal-invariant systems: $1 + 1 = 0$ mod 2.

To further determine whether SnTe or PbTe is topologically nontrivial requires looking into the microscopic band structures of SnTe and PbTe, which is beyond

the scope of the effective theory. Ab initio calculations show that the conduction (valence) band of PbTe predominantly comes from the cation Pb (the anion Te) orbitals, as expected for an ionic insulator made of Pb^{2+} and Te^{2-} in the atomic limit. In contrast, SnTe displays an anomalous band character: In a small region of the Brillouin zone around L points, the conduction (valence) band comes from the anion Te (the cation Sn) orbitals. This inverted band ordering of SnTe, distinct from an ionic insulator, is responsible for the experimentally observed decrease (increase) of band gap under tensile strain or pressure, which increases (decreases) the lattice constant towards (away from) the atomic limit. Putting together the results of the low-energy theory, topological band theory, and ab initio calculation, Hsieh et al. predicted that SnTe is a TCI, whereas PbTe is not.

2.3 Topological Crystalline Insulator Surface States

The nonzero mirror Chern number in the SnTe class of TCIs guarantees the existence of topological surface states on crystal faces that are symmetric with respect to the (110) mirror planes. Such crystal faces have a Miller index (hhk). (The cubic symmetry of SnTe dictates that the situation is the same for (khh) and (hkh) faces.) Three common surface terminations of IV-VI semiconductors are (001), (111), and (110) [see Fig. 1(a)], which all satisfy this condition. Interestingly, depending on the surface orientation, there are two types of TCI surface states, with qualitatively different electronic properties, as schematically shown in Fig. 1(b).

The first type of TCI surface states exist on the (001) and (110) surface, where a pair of L points are projected onto the same TRIMs on the surface. For the (001) surface, L_1 and L_2 are projected onto X_1, and L_3 and L_4 are projected onto X_2. In this case, the two massless surface Dirac fermions resulting from band inversions at L_1 and L_2 (L_3 and L_4) hybridize with each other at the surface and create unprecedented surface states at $\bar{X}_1$ ($\bar{X}_2$) with a double-Dirac-cone band structure. The essential properties of these surface states are captured by the following minimal $k \cdot p$ model at a given $\bar{X}$ point (41):

$$H_{\bar{X}}(\mathbf{k}) = (v_x k_x s_y - v_y k_y s_x) \otimes I + m\tau_x + \delta s_x \tau_y. \tag{3}$$

Here, the first term describes two identical copies of surface Dirac fermions associated with L_1 and L_2 (denoted by $\tau_z = \pm 1$), respectively; the other terms describe all possible inter-valley hybridizations to zeroth order in $\mathbf{k}$, which satisfy all the symmetries of the (001) surface (42, 43, 44). The calculated surface band structure of $H_{\bar{X}}$, plotted in Fig. 1(c), shows many interesting features. At low energy close to the middle of the bulk gap, the surface states consist of a pair of Dirac cones located symmetrically away from $\bar{X}$ on the line $\bar{X}\bar{\Gamma}$. The corresponding Fermi surface is two disconnected elliptical Dirac pockets. As the Fermi energy increases, these two pockets become crescent-shaped, touch each other on the line $\bar{X}\bar{M}$, and reconnect to form a large electron pocket and a small hole pocket, both centered at $\bar{X}$. This change of Fermi surface topology from be-

ing disconnected to connected, known as Lifshitz transition, leads to a Van-Hove singularity in the density of states at the transition point.

The surface band structures discussed above are directly related to the mirror Chern number of TCIs. The (001) surface exhibits surface band crossings on the line $\bar{X}\bar{\Gamma}$ between bands of opposite mirror eigenvalues, and the (111) surface shows similar crossings on the line $\bar{\Gamma}\bar{M}$. These crossings protected by mirror symmetry guarantee the gapless nature of TCI surface states, replacing the role of Kramers degeneracy in Z_2 TIs. The fact that two surface band crossings can take place at any point on the entire line agrees with the mirror Chern number $|N_M| = 2$, which precisely illustrates the principle of bulk-edge correspondence in topological phases of matter.

The second type of surface states exists on the (111) surface. Here one of the four L points in the bulk projects to the $\bar{\Gamma}$ point on the surface Brillouin zone, and the other three L points project to $\bar{M}$. As expected from the effective theory of band inversion, the (111) surface consists of four branches of massless Dirac fermions: one branch located at $\bar{\Gamma}$ and three at $\bar{M}$. Importantly, the mirror symmetry guarantees that such surface states are connected in a topologically nontrivial manner along the mirror-invariant line $\bar{\Gamma} - \bar{M}$, such that they cannot be removed. Similar to the free (111) surface, symmetry-protected interface states should exist on the (111) heterostructure between SnTe and PbTe. These interface states were anticipated from early field-theoretic studies (45, 46). The discovery of TCIs has now revealed that these states (so far unobserved) stem from the TCI material SnTe (but not PbTe) and are topologically equivalent to its (111) surface states.

2.4 Experiments

Following the prediction by Hsieh *et al.* (35) that SnTe is a TCI, angle-resolved photoemission spectroscopy (ARPES) experiments showed that SnTe (36) and $Pb_{1-x}Sn_xSe$ (37) are indeed a new type of topological materials characterized by peculiar surface states consisting of *four* Dirac cones. Later, the TCI phase was confirmed to remain in the $Pb_{1-x}Sn_xTe$ alloy for $x \gtrsim 0.25$ (38, 47). Those materials crystallize in the cubic rock-salt structure, which can be cleaved along either (001) or (111) planes. Like in Z_2 TIs, the four Dirac cones of TCIs are spin non-degenerate and are helically spin-polarized (38).

The initial experiments done on the (001) surface (36,37,38,47) found a double-Dirac-cone structure near the $\bar{X}$ point of the surface Brillouin zone [Fig. 2]. Remarkably, the Dirac points of the surface state are *not* located at the TRIMs; rather, their locations are restricted on the mirror axes of the surface Brillouin zone. Such a surface state structure stems from a mirror-symmetry-constrained hybridization of two Dirac cones (35), as described in Section 2.3. The predicted Lifshitz transition stemming from the merger of two nearby Dirac cones has also been experimentally observed (36, 37, 38).

On the (111) surface, however, all four Dirac points are located at the TRIMs: one at $\bar{\Gamma}$ and three at $\bar{M}$ points [Fig. 1(b)]. It was found both by *ab initio* calculations (41, 48) and by experiments (49) that the energy location of the

Dirac point as well as the Fermi velocity are different for the Dirac cones at $\bar{\Gamma}$ and $\bar{M}$. These two kinds of Dirac cones were found to manifest themselves in the surface transport properties as different components of the surface quantum oscillations observed in SnTe thin films grown along the [111] direction (50).

Interestingly, the difference in the Dirac cones at $\bar{\Gamma}$ and $\bar{M}$ introduces peculiar valley degrees of freedom and makes it possible to conceive unique valleytronics for the (111) surface states of TCIs (51). Another type of valley-dependent phenomenon arises on the (001) surface due to a spontaneous structural distortion that selectively breaks mirror symmetries and opens gaps at the four Dirac valleys (35). Indeed, such gap openings at two of the four Dirac cones have been observed in the Landau level map of $Pb_{1-x}Sn_xSe$ (001) surface states using scanning tunneling microscope (STM) (52).

2.5 Perturbations to the Topological Crystalline Insulator Surface States

Compared with TIs, TCI surface states have a much wider range of *tunable* electronic properties under various perturbations, such as structural distortion, magnetic dopant, mechanical strain, thickness engineering, and disorder (35, 47, 53, 54, 55, 56, 57). We now briefly discuss the interesting consequences of these perturbations on the (001) surface states, some of which have been experimentally observed.

(i) *Ferroelectric structural distortion*: A common type of structural distortion in IV-VI semiconductors is a relative displacement $\mathbf{u}$ of the cation and anion sublattices [Fig. 3(a)], which leads to a net ferroelectric polarization. Depending on the direction of $\mathbf{u}$, this distortion breaks the mirror symmetry with respect to either one or two mirror planes, and therefore generates nonzero mass for the original massless Dirac fermions on the TCI (001) surface. Both the magnitudes and the *signs* of the Dirac masses at the four valleys depend on the direction of $\mathbf{u}$, resulting in a rich phase diagram [Fig. 3(a)] (35). This Dirac mass generation by symmetry breaking has been observed in a scanning tunneling microscopy experiment on the TCI $Pb_{1-x}Sn_xSe$ (52) as already mentioned.

(ii) *Magnetic dopant*: The exchange coupling of TCI surface Dirac fermions and magnetic moments of dopants results in time-reversal-symmetry breaking. In particular, an out-of-plane magnetization opens up Zeeman gaps of the same signs at the four Dirac points, leading to quantum Hall effect with $\sigma_{xy} = 4 \times \frac{e^2}{2h}$ (35). This offers a promising route to quantum anomalous Hall states in TCI thin films, with large quantized Hall conductance (58).

(iii) *Mechanical strain*: The Dirac points on the (001) surface of TCIs are not pinned to TRIMs as in the case of TIs. In this case, a mechanical strain can shift the Dirac point positions in $\mathbf{k}$ space in a similar way as an electromagnetic gauge field acts on an electron (53). As a result, a nonuniform strain field generates a nonzero pseudo-magnetic field, that can dramatically alter the electronic properties of TCI surface states. It has been proposed (54) that a Landau-level-like flat band can be created by a periodic strain field due to the dislocation array that

spontaneously forms on the interface of TCI heterostructures, and the resulting high density of states may be responsible for the unusual interface superconductivity found in these systems (59).

(iv) *Thickness engineering*: In (001) thin films of TCIs, the top and bottom surface states hybridize to open up an energy gap at the Dirac points. However, the inverted band structure at the X points remains down to a few layers. In the wide range of intermediate thickness, these films realize a two-dimensional TCI phase that has spin-filtered edge states (55). Unlike quantum spin Hall insulators, these edge modes consist of an even number of Kramers pairs, which are protected by the symmetry with respect to the film's middle plane. Applying a small out-of-plane electric field breaks this mirror symmetry and hence gaps out these spin-filtered edge states (55). This electrically tunable edge channel may be regarded as a topological transistor, whose ON and OFF states are controlled by an electrically induced gap in the topological edge channel, instead of carrier injection/depletion (see Fig. 4).

(v) *Disorder*: Unlike internal symmetries (such as time-reversal symmetry), spatial symmetries (such as mirror symmetry) are always violated in the presence of disorder (60). This raises the question of whether TCI phases are stable against disorder. It has been argued that the topological surface states in the SnTe class of TCIs cannot be localized even under strong disorder, provided that time reversal symmetry is present (35, 57). This remarkable absence of localization is protected by the restored mirror symmetry after disorder averaging, or average mirror symmetry. Intuitively, one can treat the strongly disordered TCI surface as an ensemble of domains, where each domain breaks mirror symmetry and hence is locally gapped. However, there exist two types of domains that are related to each other by mirror symmetry. As a unique property of TCIs, the interface between the two mirror-related domains hosts a single one-dimensional helical mode (35). Since time-reversal-symmetry forbids backscattering within helical states, each domain wall is a ballistic conductor. The average mirror symmetry further guarantees that the two types of domains occur with equal probability. As a result, the conducting domain wall percolates throughout the entire surface, leading to delocalization. To make the above argument rigorous, we now present a proof (61) that in the presence of time reversal symmetry, the disordered TCI surface cannot be localized. Let us consider a setup shown in Fig. 3(b), where a disordered region of the TCI surface is confined between two gapped regions on its left and right, which are obtained by externally breaking the mirror symmetry and are swapped under mirror operation. In this setup, the disordered region is topologically equivalent to a domain wall between the two gapped regions, and hence hosts a single delocalized one-dimensional helical mode. Now suppose this disordered region could be localized, this helical mode, which cannot be "split", must sit either on the left or right boundary, which contradicts with the mirror symmetry of the entire setup. This proves by contradiction that the disordered TCI surface cannot be localized.

It is now understood that the delocalization of boundary states due to protection from an average symmetry occurs in a much broader class of topological

phases, which include for example weak topological insulators that are protected by translational symmetry (62, 63, 64, 65). Like the TCI with mirror symmetry, these topological phases (termed "statistical topological insulators" (65)) lie beyond the tenfold classification scheme (66), and have the common defining property that their boundary states exhibit two topologically distinct phases when the underlying symmetry is explicitly broken in opposite ways. It then follows from the argument presented above that when the symmetry is preserved on average, the disordered surface precisely sits at a topology-changing phase transition point and for this reason cannot be localized. The physics of such delocalization due to topology and average symmetry has been precisely formulated in a field-theoretic approach to Anderson localization (57), and confirmed in numerical studies (63, 67, 68, 69).

3 Topological Superconductor

3.1 General Concept

TSCs can be regarded as a superconducting cousin of TIs. Unlike insulators whose total number of electrons is conserved, superconductors (and superfluids) spontaneously break the $U(1)$ symmetry associated with the fermion number conservation. Instead, only the fermion number parity (i.e., even or odd) is conserved in the mean-field theory of superconductivity. This important difference in symmetry called for a new topological classification of superconductors different from insulators, which was systematically obtained in Refs. (66, 70) and led to the theoretical finding of a wide class of TSCs. Several concrete examples of TSC appeared in early models studies by Read & Green (71) and Kitaev (72), as well as others (73, 74). The search for TSCs in real materials is currently an exciting research endeavor in condensed matter physics.

A TSC is most easily conceived in a fully-gapped superconductor as one that cannot be adiabatically connected to a Bose-Einstein condensate (BEC) of Cooper pairs, in the same sense that a TI cannot be adiabatically deformed to the atomic limit. By this standard, conventional s-wave spin-singlet superconductors are clearly non-topological, because they exhibit a smooth crossover from the weak-coupling Bardeen-Cooper-Schrieffer (BCS) limit to the strong-coupling BEC limit without undergoing a gap-closing phase transition. This implies that unconventional pairing symmetry is a necessary (but not sufficient) condition for TSCs. Although the concept of TSC is most transparent in fully gapped superconductors, it is important to note that nodal (zero-gap) superconductors can also be topological as long as a topological invariant is well defined; indeed, for several particular cases of nodal superconductors, topological classifications have been accomplished and concrete topological invariants are found (75, 76).

As a consequence of its nontrivial topology, irrespective of whether it is fully gapped or nodal, a TSC is guaranteed to possess protected gapless excitations on the boundary. Importantly, unlike in TIs, these excitations are not electrons or holes (as in a normal metal) but Bogoliubov quasiparticles, namely, coherent superpositions of electrons and holes. The corresponding surface states are

Andreev bound states.

The classification of TSCs and the nature of their surface Andreev bound states depend crucially on the presence or absence of internal symmetries such as time reversal and spin rotation. Of particular interests are time-reversal-breaking TSCs (the superconducting cousin of quantum Hall insulators) and time-reversal-invariant TSCs [the superconducting analog of TIs, (77)]. A famous example of the former type is a 2D chiral $p_x + ip_y$ spin-triplet superconductor. There is evidence that an extensively studied material, Sr_2RuO_4, is a p-wave superconductor, but there is no consensus as to whether it fulfills all the requirements of a chiral TSC (78), although there is experimental indication of surface Andreev bound states (79).

In the following, we focus on time-reversal-invariant TSCs in spin-orbit-coupled systems, which have attracted wide attention only recently. Remarkably, the gapless quasiparticles on the surface of such TSCs do not carry conserved quantum numbers associated with an electron's charge or spin, and are completely indistinguishable from their antiparticles. Because particles that are their own antiparticles are called Majorana fermions (80, 81), the quasiparticles on the surface of those TSC are emergent helical Majorana fermions in the solid state, which can be thought of as one half of the helical Dirac fermion on a TI surface.

3.2 Odd-Parity Criterion

Fully gapped, time-reversal-invariant TSCs are indexed by a Z_2 topological invariant in one and two dimensions, and by an integer invariant in three dimensions (66, 70). For a given superconductor, the value of its topological index can in principle be calculated from the band structure and pair potential, using explicit but complicated formulas. Alternatively, when the superconducting energy gap Δ is much smaller than the Fermi energy μ (which holds for most known superconductors), the topological index is entirely governed by the topology of the normal-state Fermi surface and the symmetry of the superconducting order parameter, without reference to the full band structure in the Brillouin zone. As we show below, this Fermi surface and pairing-symmetry-based approach provides a straightforward criterion for TSCs that is conceptually transparent and experimentally accessible.

In particular, the criterion for time-reversal-invariant TSCs becomes remarkably simple for materials with inversion symmetry. In this case, the pairing order parameter is either even or odd parity. In the absence of spin-orbit coupling, even-parity pairing corresponds to spin-singlet pairing, whereas odd-parity pairing corresponds to spin-triplet pairing. When spin-orbit coupling is present, the notions of spin-singlet and -triplet pairing are no longer well-defined, but there remains a sharp distinction between even- and odd-parity pairings. It was found (82, 83) that even-parity pairing inevitably leads to topologically trivial superconductors, whereas odd-parity pairing leads to TSCs under broad conditions of Fermi surface topology. Specifically, when the Fermi surface encloses an odd number of TRIMs, odd-parity pairing is guaranteed to create topological superconductivity. This criterion for TSCs holds in all three spatial dimensions and

is proven by generalizing the parity criterion for TIs (9) to superconductors. In addition, 3D TSCs can also be realized when the Fermi surface encloses an even number of TRIMs, provided that the odd-parity order parameters on different Fermi pockets have the same sign (84).

The intimate connection between odd-parity pairing and topological superconductivity can be intuitively understood by analyzing the transition from the weak-coupling BCS regime to the strong-coupling BEC regime in a simple one-band system as the pairing interaction increases. Both regimes can be treated by mean-field theory. In the BCS regime, the chemical potential μ is inside the energy band and is much larger than the pairing gap, whereas in the BEC regime, μ lies below the band bottom. Therefore, the BCS-BEC transition takes place when the chemical potential (as determined self-consistently) coincides with the band edge and the Fermi surface shrinks to a point at $\mathbf{k} = 0$. Importantly, the odd-parity pair potential, a 2×2 matrix in the space of the doubly degenerate energy band, must satisfy $\Delta(\mathbf{k}) = -\Delta(-\mathbf{k})$ and hence is guaranteed to vanish at $\mathbf{k} = 0$. As a result, right at this BCS-BEC transition point, the quasiparticle dispersion becomes gapless at $\mathbf{k} = 0$. This unavoidable gap closing implies that the BCS regime of odd-parity superconductors cannot be adiabatically connected to the topological trivial BEC regime and hence must be topologically nontrivial. In contrast, for even-parity superconductors, the pairing gap $\Delta(\mathbf{k}) = \Delta(-\mathbf{k})$ can stay finite at $\mathbf{k} = 0$, and therefore the BCS regime is adiabatically connected to the BEC regime and hence is topologically trivial. This argument clearly demonstrates that odd-parity pairing is the key requirement of TSCs.

3.3 Material Proposals

Although odd-parity pairing has long been known in the context of p-wave superfluid He-3, odd-parity superconductivity is rare in solid-state systems. Prime examples are Sr_2RuO_4 (78) and certain heavy fermion superconductors [e.g., UPt_3 (85)], where the driving force for odd-parity pairing comes from the strong electron correlation in d or f orbitals. However, these odd-parity superconductors appear to break time-reversal symmetry and hence do not qualify as time-reversal-invariant TSCs.

In searching for time-reversal-invariant TSCs, Fu & Berg (82) proposed a new mechanism for odd-parity pairing facilitated by strong spin-orbit coupling, as well as a possible realization of this mechanism in a candidate material $Cu_xBi_2Se_3$. The main idea is simple: Strong spin-orbit coupling locks an electron's spin to its momentum and orbital component and thereby converts a bare interaction that is short-ranged and spin-independent to an effective interaction between Bloch electrons that is both spin- and momentum-dependent. With such a nontrivial spin- and momentum-dependence, this effective interaction is then capable of generating odd-parity superconductivity.

$Cu_xBi_2Se_3$ is a doped TI that was recently found to be superconducting, with a maximum transition temperature of 3.8 K (86). The proposed odd-parity pairing in $Cu_xBi_2Se_3$ is based on a microscopic two-orbital model of its ferminology, which also provides a minimal description of spin-orbit coupling in the presence of

inversion symmetry. Unlike the Rashba spin-splitting caused by inversion asymmetry, spin-orbit coupling in centrosymmetric materials arises from the interplay between an electron's spin, atomic orbitals, and crystalline anisotropy, and its form depends on crystal symmetry. The two relevant orbitals in $Cu_xBi_2Se_3$ are located on the upper and lower part of the quintuple layer, respectively; hence, the electronic structure can be modeled as a stack of bilayer unit cells along the z axis. On a given layer, there is a structural asymmetry between z and $-z$, which leads to a local electric field that points perpendicular to the plane in opposite directions on the top and bottom layer. This electric field generates a Rashba spin-orbit coupling associated with electron's motion within each plane,

$$H_{\rm soc} = v\sigma_z(k_x s_y - k_y s_x), \tag{4}$$

which has opposite signs for the two orbitals, labeled by $\sigma_z = \pm 1$. In addition, inter-plane hopping along the z direction connects the two orbitals in a staggered way similar to the Su-Heeger-Schrieffer model for polyacetylene. Taking both intra- and inter-plane motion into account, we arrive at the following Hamiltonian for the normal state of $Cu_xBi_2Se_3$:

$$H_{\rm 3D} = v\sigma_z(k_x s_y - k_y s_x) + v_z k_z \sigma_y + m\sigma_x, \tag{5}$$

which captures the low-energy band structure near the Γ point up to first order in $\mathbf{k}$. It is worth pointing out that apart from a change of orbital basis, the low-energy Hamiltonian Eq. (5) for $Cu_xBi_2Se_3$ takes an identical form as the Hamiltonian for SnTe, Eq. (2), because both are determined by the D_{3d} point group (or little group) of the crystal.

$Cu_xBi_2Se_3$ appears to be a weakly or moderately correlated electron system. The parent compound Bi_2Se_3 is a naturally doped semiconductor consisting of extended p-orbitals, and Cu-doping leads to a rigid-band shift of the Fermi level deeper into the conduction band. Fu & Berg (82) studied superconductivity within the two-orbital model of $Cu_xBi_2Se_3$ expressed in Eq. (5), assuming that the pairing interaction is short-ranged in space, as in the standard treatment of weak-coupling superconductors. Under this assumption, the pair potential is momentum-independent, but can have a nontrivial internal structure with spin-orbit entanglement, which is not possible in a single-orbital system. On the basis of symmetry classification, four types of such pairings were found and listed in Table 1; each one has a different symmetry corresponding to the irreducible representations of the D_{3d} point group A_{1g}, A_{1u}, A_{2u}, and E_u, respectively. The A_{1g} pairing is even parity and conventional s-wave, whereas all others are odd parity and unconventional. Specifically, the A_{2u} pairing is intra-orbital spin-singlet, but has opposite signs on the two orbitals. Both A_{1u} and E_u pairings are orbital-singlet and spin-triplet: The former has zero total spin along the z axis, whereas the latter has zero total spin along an in-plane direction, spontaneously breaking the three-fold rotation symmetry of the crystal. Because of the spin-orbit coupling, these two spin-triplet pairings are non-degenerate.

In discussing the likely pairing symmetry of $Cu_xBi_2Se_3$, Fu & Berg (82) studied the phase diagram of the two-orbital model under attractive density-density

interactions, which could come from electron-phonon coupling. The mean-field calculation showed that the s-wave pairing is favored when the intra-orbital attraction U exceeds the inter-orbital one V, whereas the odd-parity A_{1u} pairing is favored when the inter-orbital attraction is stronger. It is remarkable that unconventional odd-parity pairing can be realized in a model with purely attractive and short-range interactions, which is made possible by the strong spin-orbit interaction comparable to the Fermi energy, as one can see in Eq. (5). The requirement of $V > U$ may be achieved by taking into account the reduction of phonon-meditated attraction by renormalized Coulomb repulsion, which is larger for electrons occupying the same orbital.

The A_{1u} odd-parity pairing generates a full superconducting energy gap over the elliptical Fermi surface that encloses the time-reversal-invariant momentum Γ, thereby satisfying all the requirements for 3D time-reversal-invariant TSCs. Indeed, the A_{1u} superconducting phase supports two-dimensional massless helical Majorana fermions on the surface (82), which exhibits a novel energy-momentum dispersion (87, 88, 89). The other two odd-parity phases, A_{2u} and E_u, have point nodes. Nonetheless, both phases also have Majorana fermion surface states with Fermi arcs, whose existence is related to certain weak topological invariants (76).

3.4 Experiments and Open Issues

As is discussed above, superconductors derived from TIs are interesting candidates for bulk TSCs. Among them, the most widely studied material has been $Cu_xBi_2Se_3$, which actually provided the motivation for the Fu-Berg theory (82). The superconductivity in this material shows up as a result of Cu intercalation to the van der Waals gap of the parent Bi_2Se_3 compound (86). The bulk carrier density n_{3D} of $Cu_xBi_2Se_3$ is very low for a superconductor, $n_{3D} \simeq 1 \times 10^{20}$ cm^{-3}; for such a low carrier density, the maximum T_c of 3.8 K in $Cu_xBi_2Se_3$ is anomalously high within the context of the BCS theory, in which T_c is exponentially diminished as the density of states at the Fermi energy is reduced. As a matter of fact, the BCS theory predicts an order of magnitude lower T_c for such a low n_{3D} (90), and indeed, the prototypical low-carrier-density superconductor $SrTiO_3$ has the maximum T_c of 0.5 K for $n_{3D} \simeq 1 \times 10^{20}$ cm^{-3} (91). The anomalously high T_c for the very low carrier density is one of the possible indications of an unusual electron pairing in $Cu_xBi_2Se_3$.

Superconducting $Cu_xBi_2Se_3$ is difficult to be synthesized with the usual melt-growth technique (86), but an electrochemical technique makes it possible to synthesize samples with the superconducting volume fraction up to $\sim$70% near $x \simeq 0.3$ (92). Using such high-volume-fraction samples, it was found using specific-heat measurements that this material is likely to have a fully gapped superconducting state without gap nodes (92). More importantly, point-contact spectroscopy experiments found signatures of Andreev bound states [Fig. 5(a)], which points to the realization of unconventional odd-parity superconductivity, meaning that $Cu_xBi_2Se_3$ is a bulk TSC (75). Theoretically, the surface Andreev bound states of such a bulk TSC are nothing but the helical Majorana fermion state. Therefore, the point-contact experiments may have seen a signature of

Majorana fermions.

However, an STM study of $Cu_xBi_2Se_3$ found only a conventional tunneling spectrum (93), which created a controversy regarding the nature of superconductivity in $Cu_xBi_2Se_3$. In this context, it is worth noting that recent self-consistent calculations of the local density of states (LDOS) in $Cu_xBi_2Se_3$ concluded that the existence of the topological surface state must give rise to a two-gap structure in the LDOS spectrum at the surface if the bulk superconducting state is of the conventional BCS type (94). Therefore, it is not so straightforward to understand the STM result.

Recently, an ARPES study found that the Fermi surface of superconducting $Cu_xBi_2Se_3$ is a warped cylinder and hence the system is essentially quasi-2D (95). This result suggests the possibility that this material is actually a 2D TSC and the topological boundary states exist only on the side surface. If so, the point-contact spectroscopy using silver nanoparticles (75) could have probed the Andreev bound states at the terrace edges, whereas the STM measurements on the top surface would not probe any boundary states (94). Clearly, further studies of $Cu_xBi_2Se_3$ using different techniques, such as nuclear magnetic resonance or π junctions, are desirable for elucidating the true pairing symmetry.

Another interesting candidate of a bulk TSC is superconducting In-doped SnTe (96), which is a hole-doped TCI preserving the topological surface states even after the In doping (97). The effective Hamiltonian of this system has essentially the same form as that of the 3D version of $Cu_xBi_2Se_3$, and hence the symmetry classification of the possible gap functions in the Fu-Berg theory (82) still applies. This means that the strong spin-orbit coupling needed to make SnTe topological may also lead to unconventional superconductivity in $Sn_{1-x}In_xTe$ by promoting Cooper pairing between two different orbitals with opposite parity. Intriguingly, the point-contact spectroscopy of $Sn_{1-x}In_xTe$ found signatures of surface Andreev bound states [Fig. 5(b)] (96) similar to those found in $Cu_xBi_2Se_3$, pointing to the realization of a topological superconducting state.

It is prudent to mention that the In-doping dependence of T_c in this material is complicated (98), and it has been suggested that topological superconductivity is realized only in a narrow range of In content near 4% where disorder becomes minimal (98). The specific-heat measurements of $Sn_{1-x}In_xTe$ found that the superconducting state is fully gapped and the volume fraction is essentially 100% (98). The absence of impurity phases in $Sn_{1-x}In_xTe$ is an advantage, compared with $Cu_xBi_2Se_3$, for elucidating the nature of pairing symmetry. If the bulk is indeed topological, the surface Andreev bound states of $Sn_{1-x}In_xTe$ consist of four valleys of helical Majorana fermions because there are four bulk Fermi pockets located at the L points.

Very recently, a new TI-based superconductor, $Cu_x(PbSe)_5(Bi_2Se_3)_6$ (hereafter called CPSBS), was discovered (99). This material is interesting in that its specific-heat behavior strongly suggests the existence of gap nodes, and hence this is almost certainly an unconventional superconductor. The building block of the crystal structure of $(PbSe)_5(Bi_2Se_3)_6$ consists of two quintuple layers (QLs) of Bi_2Se_3 separated by one-unit-cell-thick PbSe, and hence it can be called a

naturally formed heterostructure of alternating topological and non-topological units; to make it a superconductor, Cu is intercalated into the van der Waals gap between the two QLs of the Bi_2Se_3 units. Although the unconventional nature in $Cu_xBi_2Se_3$ and $Sn_{1-x}In_xTe$ has so far been inferred only through the surface properties, the unconventional superconductivity in CPSBS is indicated by bulk properties [Fig. 5(c)]. This material has a quasi-2D Fermi surface, so the existence of gap nodes leads to the appearance of surface Andreev bound states on some particular planes that are parallel to the c^* axis (100). Importantly, the strong spin-orbit coupling coming from the Bi_2Se_3 unit makes the Andreev bound states spin-split and form a Kramers pair. The resulting spin-nondegenerate surface states can be identified as helical Majorana fermion states.

It is noteworthy that any spin-triplet superconductor is potentially a bulk TSC, either gapped or gapless. Hence, well-established triplet superconductors such as Sr_2RuO_4 (78) and UPt_3 (85) may well be topological, but their exact topological nature remains to be identified. Note that a topological bulk state leads to the appearance of surface Andreev bound states [Fig. 5(d), (79)] as topological gapless quasiparticle states. However, in those spin-triplet TSCs, the surface Andreev bound states may not be identified as Majorana fermion states, because they are spin degenerate; remember, two Majorana fermions with the same $\mathbf{k}$ can form a complex linear combination to result in an ordinary fermion. Nevertheless, a Majorana zero mode is expected to show up in the core of half-quantized vortices that are peculiar to triplet superconductors having the d-vector degrees of freedom (78).

4 Outlook

The discovery of TIs initiated a new trend to pursue topologically nontrivial phases in quantum materials, and one would expect this new trend to keep producing fundamental discoveries about novel quantum phases of matter characterized by nontrivial topologies. As is emphasized in the present review, important ingredients for the theoretical investigations of new types of topological materials are the construction of effective models and the symmetry analysis of such models. In this respect, theoretical imaginations to conceive exotic models are obviously important, but perhaps more important is to find/design realistic materials to realize such models so that the theoretical predictions can be verified by experiments. In any case, because topologies can only be analyzed mathematically in concrete models, the discoveries of materials characterized by new topologies are necessarily led by theoretical insights.

On the experimental front, besides exploring new kinds of topological materials, it is important to establish practical understanding of known topological materials and to elucidate peculiar phenomena associated with such materials. In this respect, the implications of the valley degrees of freedom in TCIs on various physical properties are worth pursuing. For such efforts, availability of high-quality thin films, whose Fermi level can be gate controlled, would be crucially important. Regarding TSCs, the physics of extended and dispersive Majorana

fermions on the surface of certain TSCs is a new area of research and may yield rich phenomenology, as was the case with massless Dirac fermions in graphene (101). Also, finding ways to create and manipulate a Majorana zero mode localized on a defect is important for future applications in quantum computations. Of course, before addressing such physics, the pairing symmetry of candidate TSCs derived from TIs needs to be elucidated, which is an important near-term challenge and requires further advancements in materials synthesis techniques.

On the theoretical front, classifications of possible topological phases for various symmetries will continue to be important. In particular, there are now intensive efforts on classifying and studying TCI phases protected by various crystal symmetries (102, 103, 104, 105, 106, 107, 108, 109, 110, 111, 112, 113, 114, 115, 116), as well as superconducting analogs of TCIs (117, 118, 119, 120). The role of crystal symmetry in protecting topological nodal semimetals has also been studied (121, 122, 123, 124, 125). The search for new TCI materials has attracted a great interest. Theoretically predicted or proposed candidates include heavy fermion compounds (126, 127), transition metal oxides (128), and antiperovskites (129). Regarding TSCs, mechanisms for odd-parity pairing in spin-orbit-coupled systems are being explored (130, 131, 132, 133, 134), and their unusual topological properties are being studied (135, 136, 137, 138, 139, 140, 141, 142). Importantly, the robustness of odd-parity superconductivity against disorder is found to be parametrically enhanced by strong spin-orbit coupling (143, 144). Last but not the least, a variety of new materials has recently been proposed as candidate time-reversal-invariant TSCs (145, 146, 147, 148, 149, 150), which makes this research field extremely active and lively.

Looking into the future, it remains to be seen whether strong electron correlations can give rise to novel topological phases in time-reversal-invariant systems, as was the case for fractional quantum Hall effect in time-reversal-symmetry-broken systems. In both cases, predictions of concrete candidates to realize newly conceived topological phases are crucial for advancing the physics of topological phases. To make the field of topological materials more interesting, it is desirable that experimentalists discover unexpected topological phases and phenomena in strongly correlated materials, and such serendipitous discovery would lead to a major leap in our understanding.

5 Acknowledgments

Y.A. acknowledges Kouji Segawa, Alexey Taskin, Satoshi Sasaki, Zhi Ren, Markus Kriener, Mario Novak, Fan Yang, Kazuma Eto, Takafumi Sato, Seigo Souma, Takashi Takahashi, Yukio Tanaka, and Masatoshi Sato for collaborations. L.F. thanks Arun Bansil, Erez Berg, Chen Fang, Tim Hsieh, Charlie Kane, Hsin Lin, Junwei Liu, Ling Lu, Vidya Madhavan, Karen Michaeli, Maksym Serbyn, Eveyln Tang and Ilijia Zeljkovic for collaborations, and takes this opportunity to thank Charlie Kane for introducing him to the field of topological insulators. Y.A. was supported by JSPS (KAKENHI 25220708), MEXT (Innovative Area "Topological Quantum Phenomena" KAKENHI), AFOSR (AOARD 124038). L.F. is

supported by DOE, Office of Basic Energy Science (de-sc 0010526).

Literature Cited

1. Thouless DJ, Kohmoto M, Nightingale MP, den Nijs M. 1982. *Phys. Rev. Lett.* 49:405-08.
2. Volovik GE. 2003. *The Universe in a Helium Droplet* (Oxford: Oxford University Press).
3. Kane CL, Mele EJ. 2005. *Phys. Rev. Lett.* 95:146802.
4. Bernevig BA, Hughes TL, Zhang SC. 2006 *Science* 314:1757.
5. König M, Wiedmann S, Brüne C, Roth A, Buhmann H, Molenkamp LW, Qi XL, Zhang SC. 2007. *Science* 318:766.
6. Moore JE, Balents L. 2007. *Phys. Rev. B* 75:121306.
7. Fu L, Kane CL, Mele EJ. 2007. *Phys. Rev. Lett.* 98:106803.
8. Roy R. 2009. *Phys. Rev. B* 79:195322.
9. Fu L, Kane CL. 2007. *Phys. Rev. B* 76:045302.
10. Hsieh D, Qian D, Wray L, Xia Y, Hor YS, Cava RJ, Hasan MZ. 2008. *Nature* 452:970.
11. Hasan MZ, Kane CL. 2010. *Rev. Mod. Phys.* 82:3045-67.
12. Qi X-L, Zhang S-C. 2011. *Rev. Mod. Phys.* 83:1057-110.
13. Ando Y. 2013. *J. Phys. Soc. Jpn.* 82:102001.
14. Qi X-L, Hughes TL, Zhang S-C. 2008. *Phys. Rev. B* 78:195424.
15. Fu L, Kane CL. 2008. *Phys. Rev. Lett.* 100:096407.
16. Fu L, Kane CL. 2006. *Phys. Rev. B* 74:195312.
17. Liu C, Hughes TL, Qi XL, Wang K, Zhang SC. 2008. *Phys. Rev. Lett.* 100:236601.
18. Knez I, Du RR, Sullivan G. 2011. *Phys. Rev. Lett.* 107:136603.
19. Nishide A, Taskin AA, Takeichi Y, Okuda T, Kakizaki A, et al. 2010. *Phy. Rev. B* 81:041309.
20. Zhang HJ, Liu CX, Qi XL, Dai X, Fang Z, Zhang SC. 2009. *Nat. Phys.* 5:438.
21. Chen YL, Analytis JG, Chu JH, Liu ZK, Mo SK, et al. 2009. *Science* 325:178.
22. Xia Y, Qian D, Hsieh D, Wray L, Pal A, et al. 2009. *Nat. Phys.* 5:398.
23. Ren Z, Taskin AA, Sasaki S, Segawa K, Ando Y. 2010. *Phys. Rev. B* 82:241306(R).
24. Xiong J, Petersen AC, Qu D, Cava RJ, Ong NP. 2012. *Physica E* 44:917.
25. Ren Z, Taskin AA, Sasaki S, Segawa K, Ando Y. 2011. *Phys. Rev. B* 84:165311.
26. Taskin AA, Ren Z, Sasaki S, Segawa K, Ando Y. 2011. *Phys. Rev. Lett.* 107:016801.
27. Brüne C, Liu CX, Novik EG, Hankiewicz EM, Buhmann H, et al. 2011. *Phys. Rev. Lett.* 106:126803.
28. Zhang J, Chang CZ, Zhang Z, Wen J, Feng X, et al. 2011. *Nat. Commun.* 2:574.
29. Kim D, Cho S, Butch NP, Syers P, Kirshenbaum K, et al. 2012. *Nat. Phys.* 8:459.

30. Gu Z-C, Wen X-G. 2009. *Phys. Rev. B* 80:155131.
31. Senthil T, arXiv:1405.4015 (to appear in Annual Review of Condensed Matter)
32. Fu L. 2011. *Phys. Rev. Lett.* 106:106802.
33. Teo JCY, Fu L, Kane CL. 2008. *Phys. Rev. B* 78: 045426.
34. Mong RSK, Essin AM, Moore JE. 2010. *Phys. Rev. B.* 81:245209.
35. Hsieh TH, Lin H, Liu J, Duan W, Bansil A, Fu L. 2012. *Nature Commun.* 3:982.
36. Tanaka Y, Ren Z, Sato T, Nakayama K, Souma S, Takahashi T, Segawa K, Ando Y. 2012. *Nat. Phys.* 8:800.
37. Dziawa P, Kowalski BJ, Dybko K, Buczko R, Szczerbakow A, et al. 2012. *Nat. Mater.* 11:1023.
38. Xu SY, Liu C, Alidoust N, Neupane M, Qian D, et al. 2012. *Nat. Commun.* 3:1192.
39. Mitchell DL, Wallis RF. 1966. *Phys. Rev.* 151: 581595.
40. Dimmock JO., Melngailis I. and Strauss, AJ. 1966. *Phys. Rev. Lett.* 16:1193.
41. Liu J, Duan W, Fu L. 2013. *Phys. Rev. B* 88: 241303(R).
42. Fang C, Gilbert MJ, Xu S, Bernevig BA, Hasan MZ. 2013. *Phys. Rev. B* 88:125141.
43. Wang YJ, Tsai WF, LinH , Xu S, Neupane M, Hasan MZ, Bansil A. 2013. *Phys. Rev. B* 87:235317.
44. Takahashi R, Murakami S. 2011. *Phys. Rev. Lett.* 107:166805.
45. Volkov BA., Pankratov, OA. 1985, *JETP Lett.* 42:178.
46. Fradkin, EF., Dagotto E., and Boyanovsky, D. 1986, *Phys. Rev. Lett.* 5:2967.
47. Tanaka Y, Sato T, Nakayama K, Souma S, Takahashi T, Ren Z, Novak M, Segawa K, Ando Y. 2013. *Phys. Rev. B* 87:155105.
48. Safaei S, Kacman P, Buczko R. 2013. *Phys. Rev. B* 88:045305.
49. Tanaka Y, Shoman T, Nakayama K, Souma S, Sato T, Takahashi T, Novak M, Segawa K, Ando Y. 2013. *Phys. Rev. B* 88:235126.
50. Taskin AA, Yang F, Sasaki S, Segawa K, Ando Y. 2014. *Phys. Rev. B* 89:121302.
51. Ezawa M. 2014. *New J. Phys.* 16:06501.
52. Okada Y, Serbyn M, Lin H, Walkup D, Zhou W, et al. 2013. *Science* 341:1496-9.
53. Serbyn M, Fu L. 2014. *Phys. Rev. B* 90:035402.
54. Tang E, Fu L. 2014. *Nat. Phys.* 10:964.
55. Liu J, Hsieh TH, Wei P, Duan W, Moodera J, et al. 2014. *Nat. Mater.* 13:178-83.
56. Qian X, Fu L, Li J. 2014. Nano Res. DOI:10.1007/s12274-014-0578-9.
57. Fu L, Kane CL. 2012. *Phys. Rev. Lett.* 109:246605.
58. Fang C, Gilbert MJ, Bernevig BA. 2014. *Phys. Rev. Lett.* 112:046801.
59. Yuzephovich OI, Mikhailov MY, Bengus SV, Aladyshkin AY, Pestov EE, et al. 2008. *Low Temp. Phys.* 34:985.
60. Ludwig AWW, Fisher MPA, Shankar R, Grinstein G. 1994. *Phys. Rev. B* 50:7526-52.

61. Fu L. 2013, lecture on 7th ISSP International Workshop on Emergent Quantum Phases in Condensed Matter, `http:www.issp.u-tokyo.ac.jp/public/EQPCM/program/ws/3_Fu.pdf`
62. Ringel Z, Kraus YE, Stern A 2012. *Phys. Rev. B* 86:45102.
63. Mong RSK, Bardarson JH and Moore JE. 2012. *Phys. Rev. Lett.* 108:076804.
64. Liu CX, Qi XL and Zhang SC. 2012, *Physica E* 44:906.
65. Fulga IC, van Heck B, Edge JM, Akhmerov AR. 2014. *Phys. Rev. B* 89:155424.
66. Schnyder AP, Ryu S, Furusaki A, Ludwig AWW. 2008. *Phys. Rev. B* 78:195125.
67. Obuse H, Ryu S, Furusaki A and Murphy C 2014. *Phys. Rev. B* 89:155315.
68. Kobayashi K, Ohtsuki T, Imura K 2013. *Phys. Rev. Lett.* 110:236803.
69. Baireuther B, Edge JM, Fulga IC, Beenakker CWJ. 2014. *Phys. Rev. B* 89:035410.
70. Kitaev A. 2009. arXiv:0901.2686.
71. Read N, Green D. 2000. *Phys. Rev. B* 61:10267.
72. Kitaev A. 2000. arXiv:cond-mat/0010440.
73. Qi XL, Hughes TL, Raghu S, Zhang SC. 2009 *Phys. Rev. Lett.* 102:187001.
74. Roy R. 2008. arXiv:0803.2868
75. Sasaki S, Kriener M, Segawa K, Yada K, Tanaka Y, et al. 2011. *Phys. Rev. Lett.* 107:217001.
76. Sato M, Fujimoto S. 2010. *Phys. Rev. Lett.* 105:217001.
77. Qi X-L, Hughes TL, Raghu S, Zhang S-C. 2009. Phys. Rev. Lett. 102:187001.
78. Maeno Y, Kittaka S, Nomura T, Yonezawa S, Ishida K. 2012. *J. Phys. Soc. Jpn.* 81:011009.
79. Kashiwaya S, Kashiwaya H, Kambara H, Furuta T, Yaguchi H, et al. 2011. *Phys. Rev. Lett.* 107:077003.
80. Alicea J. 2012. *Rep. Prog. Phys.* 75:076501.
81. Beenakker CWJ. 2013. *Annu. Rev. Condens. Mat. Phys.* 4:113.
82. Fu L, Berg E. 2010. *Phys. Rev. Lett.* 105:097001.
83. Sato M. 2010. *Phys. Rev. B* 81:220504(R).
84. Qi Y, Fu L. 2012. APS March meeting, sesion Z31.00003: "Theory of Odd-Parity Superconductivity: from Gap Function to Topological Invariants and Surface Andreev Bound States".
85. Joynt R, Taillefer L. 2002. *Rev. Mod. Phys.* 74:235-94.
86. Hor YS, Williams AJ, Checkelsky JG, Roushan P, Seo J, et al. 2010. *Phys. Rev. Lett.* 104:057001.
87. Hsieh TH, Fu L. 2012. *Phys. Rev. Lett.* 108:107005.
88. Hao L, Lee TK. 2011. *Phys. Rev. B* 83:134516.
89. Yamakage A, Yada K, Sato M, Tanaka Y. 2012. *Phys. Rev. B* 85:180509(R).
90. Cohen ML, in Superconductivity, edited by Parks RD (Marcel Dekker, New York, 1969), Vol. 1, chap. 12, pp. 615-664.
91. Schooley JF, Hosler WR, Embler E, Becker JH, Cohen ML, Koonce CS. 1965. *Phys. Rev. Lett.* 14:305.
92. Kriener M, Segawa K, Ren Z, Sasaki S, Ando Y. 2011. *Phys. Rev. Lett.*

106:127004.
93. Levy N, Zhang T, Ha J, Sharifi F, Talin AA, et al. 2013. *Phys. Rev. Lett.* 110:117001.
94. Mizushima T, Yamakage A, Sato M, Tanaka Y. 2014. *Phys. Rev. B* 90:184516..
95. Lahoud E, Maniv E, Petrushevsky MS, Naamneh M, Ribak A, et al. 2013. *Phys. Rev. B* 88:195107.
96. Sasaki S, Ren Z, Taskin AA, Segawa K, Fu L, Ando Y. 2012. *Phys. Rev. Lett.* 109:217004.
97. Sato T, Tanaka Y, Nakayama K, Souma S, Takahashi T, Segawa K, Ando Y. 2013. *Phys. Rev. Lett.* 110:206804.
98. Novak M, Sasaki S, Kriener M, Segawa K, Ando Y. 2013. *Phys. Rev. B* 88:140502.
99. Sasaki S, Segawa K, Ando Y. 2014. *Phys. Rev. B* 90:184516.
100. Satoshi K, Yukio T. 2000. *Rep. Prog. Phys.* 63:1641-724.
101. Castro Neto AH, Peres NMR, Novoselov KS, Geim AK. 2009. *Rev. Mod. Phys.* 81:109-62.
102. Fang C., Gilbert MJ and Bernevig BA. 2012, *Phys. Rev. B* 86:115112.
103. Slager R., Mesaros A., Juricic V. and Zaanen J., 2013, *Nat. Phys.* 9:2513.
104. Chiu CK, Yao H, Ryu S, 2013. *Phys. Rev. B* 88:075142.
105. Taherinejad M, Garrity KF, Vanderbilt D, 2014, *Phys. Rev. B* 89:115102.
106. Morimoto T. and Furusaki, A. 2013. *Phys. Rev. B* 88:125129.
107. Jadaun P., Xiao D., Niu Q. and Banerjee, SK. 2013. *Phys. Rev. B* 88:085110.
108. Fang C., Gilbert MJ, and Bernevig BA 2013, *Phys. Rev. B* 88:085406.
109. Alexandradinata A., Fang C., Gilbert MJ. Bernevig BA. 2014. *Phys. Rev. Lett.* 113:116403.
110. Arrachea L and Aligia A. 2014, *Phys. Rev. B* 90:125101.
111. Lu YM and Lee DH. 2014, arXiv:1403.5558.
112. Liu CX, Zhang RX and BanLeeuwen K. 2014. *Phys. Rev. B* 90:085304.
113. M. Kindermann. 2013, arXiv:1309.1667.
114. Liu CX and Zhang RX. 2014, arXiv:1401.6922.
115. Liu CX. 2013, arXiv: 1304.6455.
116. Shiozaki K and Sato M. 2014. *Phys. Rev. B* 90:165114.
117. Teo JCY and Hughes TL. 2013. *Phys. Rev. Lett.* 111:047006.
118. Fang C, Gilbert MJ and Bernevig BA. 2014. *Phys. Rev. Lett.* 112:106401.
119. Benalcazar WA, Teo JCY and Hughes TL. 2014. *Phys. Rev. B* 89:224503.
120. Mizushima T, Tsutsumi Y, Sato M and Machida K. 2014. arXiv:1409.6094.
121. Yang BJ, Nagaosa N 2014, *Nature Commun.*, 5:4989.
122. Koshino M., Morimoto T., Sato M. 2014. *Phys. Rev. B* 90:115207.
123. Chiu CK and Schnyder AP, 2014, *Phys. Rev. B* 90:205136.
124. Ezawa M. 2014. arXiv:1406.1009.
125. Chen Y, Lu YM and Kee HY. 2014. arXiv:1410.5830.
126. Weng H, Zhao J., Wang Z, Fang Z. and Dai X. 2014. *Phys. Rev. Lett.* 112:016403.
127. Ye M, Allen JW, Sun K 2014. arXiv:1307.7191.

128. Kargarian M. and Fiete GA. 2013. *Phys. Rev. Lett.* 110:156403.
129. Hsieh TH, Liu JW and Fu L. 2014. *Phys. Rev. B* 90:08112(R).
130. Wan X and Savrasov SY. 2014, *Nat. Comm.* 5:4144.
131. Roy B, Sau JD and Das Sarma, S. 2014, *Phys. Rev. B* 89: 165119.
132. Brydon PMR, Das Sarma, SD, Hui HY and Sau JD. 2014. *Phys. Rev. B* 90:184512.
133. Hao L, Wang GL, Lee TK, Wang J, Tsai WF and Yang YH. 2014. *Phys. Rev. B* 89:214505.
134. Rosenstein B, Shapiro BY, Li D and Shapiro I. 2015. *J. Phys: Condens. Matter* 27:025701.
135. Ryu S, Moore JE, and Ludwig AWW. 2012. *Phys. Rev. B* 85: 045104.
136. Nomura K, Ryu S, Furusaki A and Naogaosa N. 2012. *Phys. Rev. Lett.* 108:026802.
137. Keselman A, Fu L, Stern A and Berg E. 2013. *Phys. Rev. Lett.* 111: 116402.
138. Zhang F, Kane CL and Mele EJ. 2013. *Phys. Rev. Lett.* 111:056402
139. Lawson BJ, Hor YS and Li L. 2012. *Phys. Rev. Lett.* 109:226406.
140. Qi XL, Witten E and Zhang SC. 2013. *Phys. Rev. B.* 87:134519.
141. Yip SK. 2013. *Phys. Rev. B* 87:104505.
142. Fu L. 2014. *Phys. Rev. B* 90:100509(R).
143. Michaeli K and Fu L. 2012. *Phys. Rev. Lett.* 109:187003.
144. Nagai Y, Ota Y and Machida M. 2014. *Phys. Rev. B* 89:214506.
145. Nakosai N, Tanaka Y and Nagaosa N. 2012. *Phys. Rev. Lett.* 108:147003.
146. Xiang YY, Wang WS, Wang QH and Lee DH. 2012. *Phys. Rev. B* 86, 024523.
147. Wang J, Xu Y and Zhang SC. 2014. *Phys. Rev. B* 90: 054503.
148. Scheurer M and Schmalian J. 2014. *arXiv:1404.4039*
149. Qi XL, Hughes TL and Zhang SC. 2010. *Phys. Rev. B* 81:134508.
150. Hosur P, Dai X, Fang Z and Qi XL. 2014. *Phys. Rev. B* 90: 045130.

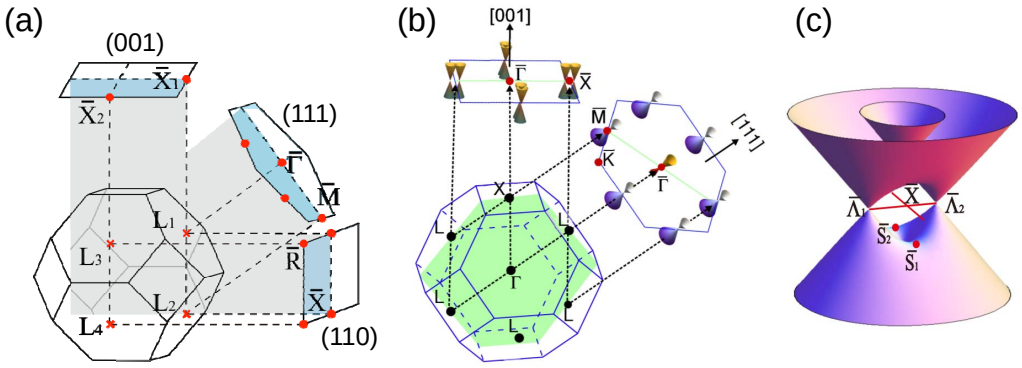

Figure 1: Topological crystalline insulator (TCI). (a) High-symmetry points in the 3D Brillouin zone and in the projected surface Brillouin zone for three different surfaces of the rock-salt crystal structure. Adapted from Ref. (41); copyright (2013) by the American Physical Society. (b) Locations of the Dirac cones in the (111) and (001) surface Brillouin zone. (c) Result of the tight-binding calculations for the dispersion of the (001) double-Dirac-cone surface state. Adapted from Ref. (41); copyright (2013) by the American Physical Society.

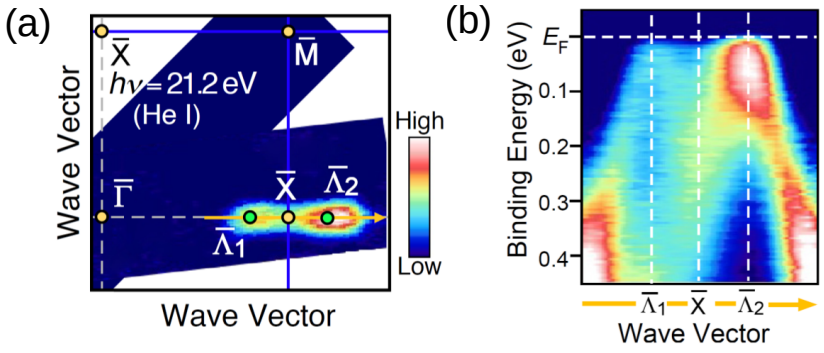

Figure 2: Double-Dirac-cone surface state observed by angle-resolved photoemission spectroscopy (ARPES) experiments on SnTe. (a) Distribution of the ARPES intensity at the Fermi energy E_F in the Brillouin zone (k_x vs k_y). (b) The dispersion relations $E(k)$ when taken as a slice through the Fermi surface found in panel (a); this slice is taken along the yellow arrow indicated in panel (a). Adapted from Ref. (36).

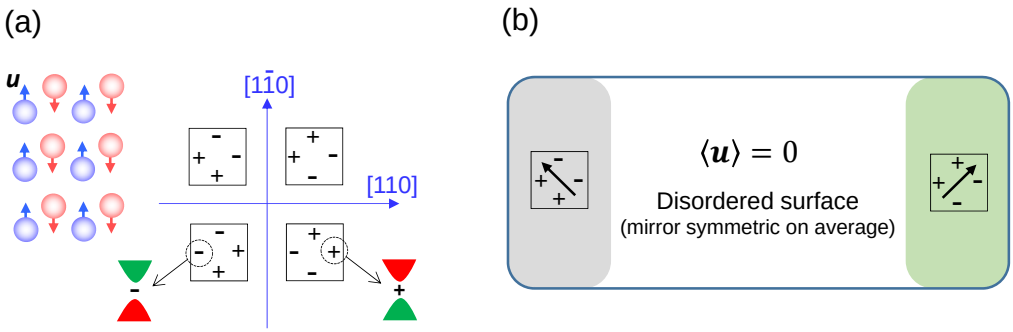

Figure 3: (a) Dirac mass generation due to ferroelectric structural distortion for the SnTe-class of TCI materials. Both the magnitude and the sign of the Dirac masses depend on the direction of the distortion **u**, as depicted in the figure. (b) Schematic picture to depict the robustness of the TCI surface states against disorder; if disordered surface were localized, there must be one helical mode localized on either left or right boundary of the central disordered region, which would contradict mirror symmetry.

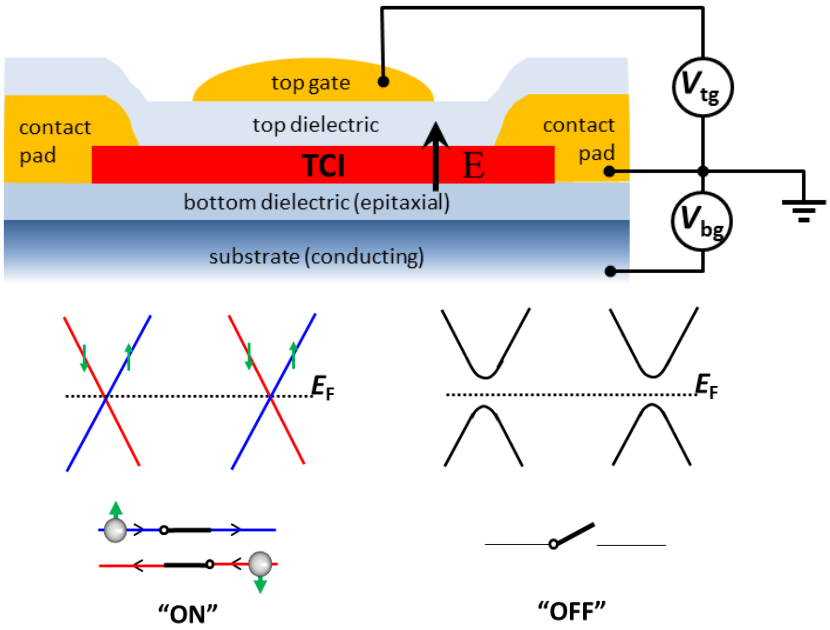

Figure 4: Possible TCI device to switch on and off the topological conduction channel with electric field which breaks mirror symmetry with respect to the film's middle plane. Adapted from Ref. (55).

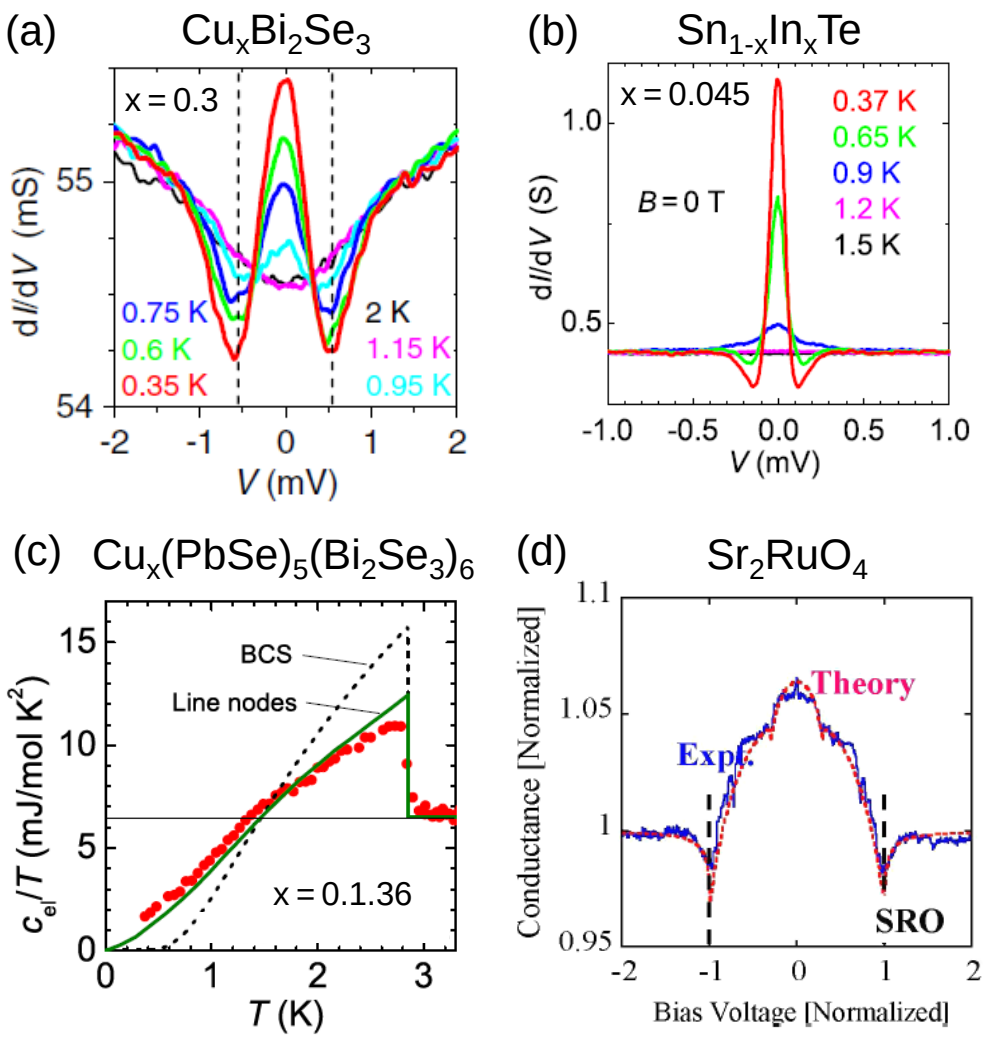

Figure 5: Experiments on topological superconductor (TSC) candidates. (a) Zero-bias conductance peak observed in a point-contact spectroscopy of $Cu_xBi_2Se_3$, which points to the existence of surface Andreev bound states and makes this material a prime candidate of the time-reversal-invariant TSC. Adapted from Ref. (75); copyright (2011) by the American Physical Society. (b) Zero-bias conductance peak observed in the point-contact spectroscopy of $Sn_{1-x}In_xTe$, which is another candidate of the time-reversal-invariant TSC. Adapted from Ref. (96); copyright (2012) by the American Physical Society. (c) Temperature dependence of the electronic specific-heat of a recently-discovered superconductor, $Cu_x(PbSe)_5(Bi_2Se_3)_6$ (CPSBS), which presents strong bulk signatures of unconventional superconductivity with gap nodes. Adapted from Ref. (99); copyright (2014) by the American Physical Society. (d) Zero-bias conductance peak observed in a tunneling spectroscopy of Sr_2RuO_4, which is a prime candidate of the time-reversal-breaking chiral TSC; calculated spectrum originating from the surface Andreev bound state is also shown. Reprinted with permission from Ref. (79); copyright (2011) by the American Physical Society.

Types of pairing in terms of field operators	Rep.	P	C_3	M
$\Delta_1:\ c^\dagger_{1\uparrow}c^\dagger_{1\downarrow}+c^\dagger_{2\uparrow}c^\dagger_{2\downarrow};\ c^\dagger_{1\uparrow}c^\dagger_{2\downarrow}-c^\dagger_{1\downarrow}c^\dagger_{2\uparrow}$	A_{1g}	$+$	$+$	$+$
$\Delta_2:\ c^\dagger_{1\uparrow}c^\dagger_{2\downarrow}+c^\dagger_{1\downarrow}c^\dagger_{2\uparrow}$	A_{1u}	$-$	$+$	$-$
$\Delta_3:\ c^\dagger_{1\uparrow}c^\dagger_{1\downarrow}-c^\dagger_{2\uparrow}c^\dagger_{2\downarrow}$	A_{2u}	$-$	$+$	$+$
$\Delta_4:\ (ic^\dagger_{1\uparrow}c^\dagger_{2\uparrow}-ic^\dagger_{1\downarrow}c^\dagger_{2\downarrow}, c^\dagger_{1\uparrow}c^\dagger_{2\uparrow}+c^\dagger_{1\downarrow}c^\dagger_{2\downarrow})$	E_u	$(-,-)$	(x,y)	$(+,-)$

Table 1: Four types of on-site pairing order parameters in the two-orbital model for $Cu_xBi_2Se_3$, which belong to the A_{1g}, A_{1u}, A_{2u} and E_u irreducible representations of the D_{3d} point group, as well as their transformation properties under point group symmetry operations. Adapted from Ref. (82). (Abbreviation: Rep., representation)